scientific reports

Check for updates

OPEN

Human psychophysical discrimination of spatially dependant Pancharatnam–Berry phases in optical spin-orbit states

D. Sarenac[1]✉, A. E. Silva[2], C. Kapahi[1,3], D. G. Cory[1,4], B. Thompson[2,5] & D. A. Pushin[1,3]

We tested the ability of human observers to discriminate distinct profiles of spatially dependant geometric phases when directly viewing stationary structured light beams. Participants viewed polarization coupled orbital angular momentum (OAM) states, or "spin-orbit" states, in which the OAM was induced through Pancharatnam–Berry phases. The coupling between polarization and OAM in these beams manifests as spatially dependant polarization. Regions of uniform polarization are perceived as specifically oriented Haidinger's brushes, and study participants discriminated between two spin-orbit states based on the rotational symmetry in the spatial orientations of these brushes. Participants used self-generated eye movements to prevent adaptation to the visual stimuli. After initial training, the participants were able to correctly discriminate between two spin-orbit states, differentiated by OAM = ±1, with an average success probability of 69% (*S.D.* = 22%, $p = 0.01$). These results support our previous observation that human observers can directly perceive spin-orbit states, and extend this finding to non-rotating beams, OAM modes induced via Pancharatnam–Berry phases, and the discrimination of states that are differentiated by OAM.

The phase that is acquired during cyclic evolution governed by a slow change of parameters is known as the geometric phase[1]. The Aharonov–Bohm phase in quantum mechanics[2] and the Pancharatnam–Berry phase in optics[3,4] are the two of the most well-known examples of phase shifts with geometrical origin, and they have had a profound impact on a wide range of areas in physics[5–8]. Unlike typical phase shifts that arise from optical path differences, the Pancharatnam–Berry phase is induced when the polarization state traces out a geodesic triangle on the Poincaré sphere[3,4]. It has led to the development of optical components that enable polarization dependant wavefront shaping and novel methods of inducing polarization coupled orbital angular momentum (OAM) through spin-orbit coupling[9–14]. Optical waves carrying OAM possess a helical wavefront and are described by the phase term $e^{i\ell\phi}$, where ϕ is the azimuthal coordinate and ℓ is the OAM value[15]. Beams with polarization coupled OAM, also known as "vector vortex beams" or "spin-orbit" beams, may be prepared to be non-separable in polarization and spatial modes[16,17] and manifest dynamic 2D polarization topologies[18–21]. A variety of methods exist to generate spin-orbit beams using spatial light modulators[22,23], sub-wavelength gratings[24], and inter-cavity interference within a laser source[25,26].

Due to their unique propagation properties spin-orbit beams have found numerous applications in high-resolution imaging, communication protocols, and optical metrology[27–29] and a wealth of characterization techniques based on Stokes polarimetry have been developed[30–32]. Ref.[33] extended the applications to visual science which sees a growing interest in integrating human detectors with recent technological advances[34–38]. It was shown that humans are able to perceive and discriminate spin-orbit states through entoptic images that arise from the interaction between the 2D polarization topologies of these beams and the radially symmetric dichroic elements in the macula of the human eye[33]. As shown in Fig. 1a, when looking in the vicinity of the center of a spin-orbit beam composed of a superposition of right and left circular polarization coupled to two different OAM values (ℓ_1 and ℓ_2), the observer may perceive an entoptic profile composed of $N = |(\ell_1 - \ell_2) - 2|$ azimuthal fringes. Note that this is a measurement of the OAM difference between the two polarization states, rather than the

[1]Institute for Quantum Computing, University of Waterloo, Waterloo, ON N2L3G1, Canada. [2]School of Optometry and Vision Science, University of Waterloo, Waterloo, ON N2L3G1, Canada. [3]Department of Physics and Astronomy, University of Waterloo, Waterloo, ON N2L3G1, Canada. [4]Department of Chemistry, University of Waterloo, Waterloo, ON N2L3G1, Canada. [5]Centre for Eye and Vision Research, 17W Science Park, Hong Kong. ✉email: dsarenac@uwaterloo.ca

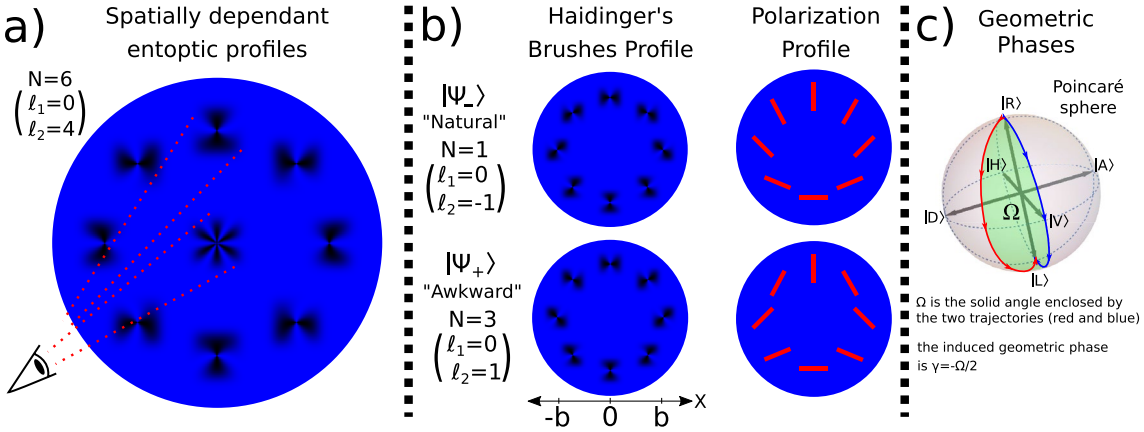

Figure 1. (**a**) Pictorial representation of the spatially dependant entoptic profiles that a human observer would perceive when directly viewing different regions of a spin-orbit beam described by Eq. (1) where $\ell_1 = 0$ and $\ell_2 = 4$. If the observer looks at the polarization gradient in the center they will perceive $|(\ell_1 - \ell_2) - 2| = 6$ azimuthal fringes. If the observer looks at a region away from the center where the polarization is roughly uniform in the field of vision, they will observe specifically oriented Haidinger's brushes. (**b**) In this study the strong polarization gradients in the central region of the beam were reduced by preparing spin-orbit states with radially dependent terms, as described by Eq. (2). The distance at which there is an equal amount of the two circular polarization states is denoted by b, and in our particular setup b was approximately 1.5 cm. The beam state was not varied with time, and the participants were asked to move their gaze around the perimeter of the beam while observing and discriminating the elicited Haidinger's brush profile, labelled either the "awkward" or "natural" profile depending on whether the entoptic brush appeared to rotate along or against the observer's eye movement. In order to minimize visual adaptation to optical polarization the suggested speed for the self-generated circular eye motion was 1 Hz. (**c**) To visually depict the role of the geometric phases in the preparation of the shown profiles, we can map the evolution of polarization from r = 0 to r = 2b (from $|R\rangle$ to $|L\rangle$) onto the Poincaré sphere[39,40]. The geometric phase is given by $\gamma = -\Omega/2$, where Ω is the solid angle enclosed by two trajectories. Considering that in the preparation of the shown polarization profiles the azimuthal coordinate ϕ determines the angle between the corresponding trajectories on the Poincaré sphere, it follows that the geometric phase gives rise to an OAM term $e^{\pm i\phi}$ coupled to the $|L\rangle$ component of $|\Psi_\pm\rangle$.

absolute value of each OAM component. Ref.[33] employed refractive elements to generate OAM = 7 and couple it to different polarization states to induce $N = 5$ and $N = 9$ azimuthal fringes. Here we consider spin-orbit states prepared through devices that manipulate geometric phases. This enables a robust study of discriminating between beams with different OAM values.

The detection of optical polarization by humans is enabled by a series of radially symmetric dichroic elements centred on the foveola in the human eye[41–45]. An observer directly viewing polarized light would perceive a bowtie-like shape, known as "Haidinger's brush", in the central point of their visual field. These entoptic profiles can be observed, on average, in light with more than approximately 56% polarization[46], with peak clarity occurring for blue light of approximately 460 nm wavelength[47]. However, observation of Haidinger's brush in everyday life is hindered by visual adaptation which causes the entoptic images to disappear after a few seconds. Experiments show that a rotating polarization source at approximately 1 Hz allows Haidinger's brush to be observed continuously with clarity[48].

Typical studies with human detectors of optical polarization require the observer to keep their gaze on a fixed point while the beam is time modulated to overcome visual adaptation. Correspondingly, in Ref.[33] an induced phase shift caused the entoptic profile to rotate. In the presented study we consider an alternative method of observation utilizing stationary beams. Rather than fixing their gaze at the center of the beam, the participants made self-generated eye movements to view different parts of the beam and determine the presented state based on the rotational symmetry of the Haidinger's brushes (see Fig. 1b).

The transverse wavefunction of a spin-orbit state travelling along the z-direction can be written as:

$$|\Psi\rangle = \frac{1}{\sqrt{2}}\left[C_1(\ell_1, r, z)e^{i\ell_1\phi}|R\rangle + C_2(\ell_2, r, z)e^{i\ell_2\phi}|L\rangle\right], \tag{1}$$

where we have used the bra-ket notation for convenience, $|L\rangle = \begin{pmatrix}0\\1\end{pmatrix}$ and $|R\rangle = \begin{pmatrix}1\\0\end{pmatrix}$ denote the left and right circular polarization, and (r, ϕ) are the cylindrical coordinates. The radial terms $C_1(\ell_1, r, z)$ and $C_2(\ell_2, r, z)$ depend on the preparation method[15,49].

In our setup the spin-orbit states were prepared via Lattice of Optical Vortices (LOV) prism pairs which induce highly uniform phase gradients and minimize distortions in the beam's intensity profile[50–52]. Furthermore, they introduce a radial dependence which can be used to prepare a cue that helps participants learn the proper eye movement. In the study we specifically prepare and differentiate between the following two states:

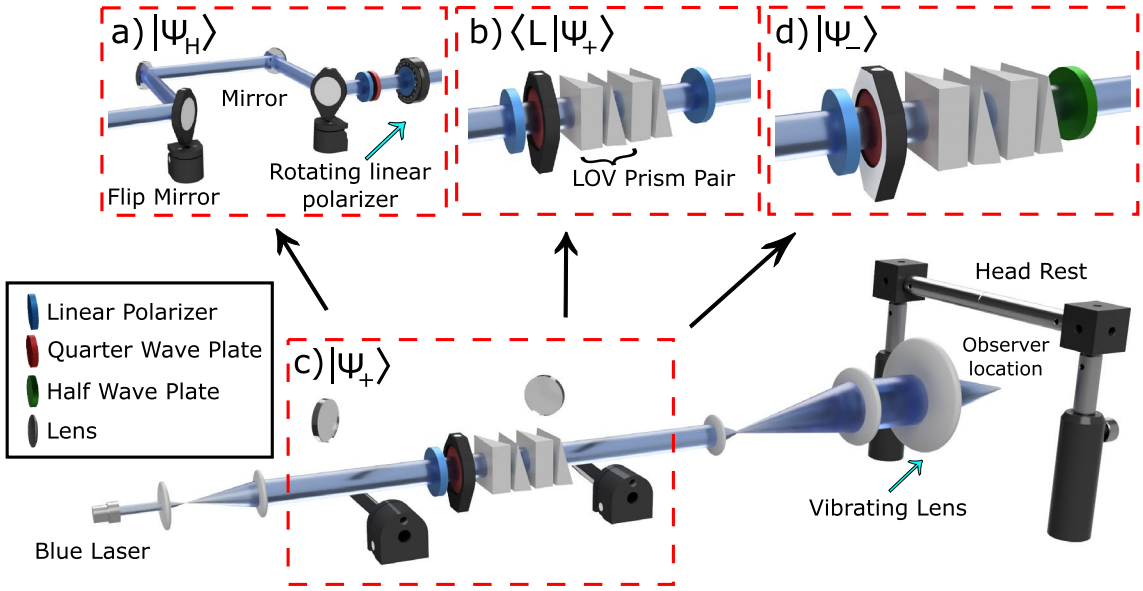

Figure 2. Schematic of the experimental setup with four different configurations for directing structured light onto the retina of the observer. (**a**) The first configuration prepares linearly polarized light with an orientation that rotates with a speed of approximately 1 Hz. This setup was used in the pre-study to determine if the participants were able to perceive Haidinger's brushes when gazing at a fixed point. (**b**) The second configuration uses a polarization filter to prepare a doughnut shaped intensity profile. This configuration was used to familiarize the participant with the optimal eye movement during a familiarization period on the first day. The last two configurations, (**c**,**d**), prepare the two states of Eq. (2) which possess uniform intensity profiles and were used during the main experiment.

$$|\Psi_{\pm}\rangle \approx \cos\left(\frac{\pi r}{4b}\right)|R\rangle \pm i \sin\left(\frac{\pi r}{4b}\right) e^{\pm i\phi}|L\rangle, \tag{2}$$

where b is the distance at which there is an equal amount of the two circular polarization states. The helical phase denoting the OAM is induced via the Pancharatnam–Berry phases (see Fig. 1c). It follows from Eq. (2) that the left circular polarization state of $|\Psi_+\rangle$ carries an OAM of +1 and that of $|\Psi_-\rangle$ carries an OAM of −1. Polarization directions, and the orientations of the corresponding Haidinger's brushes, are shown in Fig. 1b for several regions centered on $r = b$. Viewing slightly different radii would result in the same rotational symmetry but with reduced contrast. Note that the polarization topologies of $|\Psi_+\rangle$ and $|\Psi_-\rangle$ depict the "star" and "lemon" Poincaré beams[18–21].

The OAM dynamics were negligible and the beams possessed highly uniform intensity profiles in our setup. As a result, a speckle pattern arose which greatly hindered the observation of entoptic images. Therefore, we employed a vibrating lens, which is a common method of removing speckle patterns[53].

In typical operation two sets of LOV prism pairs take as input a circularly polarized state and output a lattice of spin-orbit states. The parameters in the experiment were such that one unit cell covered the entire beam, and the state in each unit cell of the lattice depended on the polarization of the input state as follows:

$$|R\rangle \rightarrow \cos\left(\frac{\pi r}{4b}\right)|R\rangle + i \sin\left(\frac{\pi r}{4b}\right) e^{i\phi}|L\rangle \tag{3}$$

$$|L\rangle \rightarrow \cos\left(\frac{\pi r}{4b}\right)|L\rangle + i \sin\left(\frac{\pi r}{4b}\right) e^{-i\phi}|R\rangle \tag{4}$$

It follows that $|\Psi_+\rangle$ may be obtained by passing $|R\rangle$ through two sets of LOV prism pairs, while to obtain $|\Psi_-\rangle$ we start with an input of $|L\rangle$ and add a half wave plate at the end.

Our setup allowed for the robust and quick access to four different configurations, as shown in Fig. 2. For a detailed description of the setup see Supplementary Material A and B, including the polarization analysis of the beam profile using the Stokes parameters[54] and the laser safety considerations[55]. The first configuration, Fig. 2a, prepares a uniform intensity beam with a varying linear polarization direction:

$$|\Psi_{\mathrm{H}}\rangle \approx |R\rangle + e^{i\theta(t)}|L\rangle, \tag{5}$$

where $\theta(t)$ was set by the rotation stage onto which a polarizer was mounted. This configuration was used in the study for pre-screening of the participants. The second configuration prepares the $|\Psi_+\rangle$ state (described by Eq. (2)) filtered on $|L\rangle$. The resulting intensity possesses a doughnut profile that is described by $\sin^2(\pi r/4b)$. The outer boundary of the central dark region provides an aligning aid for participants, outlining the optimal locations for saccadic eye movements when discriminating the spin-orbit states. This configuration was used during an initial familiarization and training period. The third and fourth configurations are the $|\Psi_+\rangle$ and $|\Psi_-\rangle$

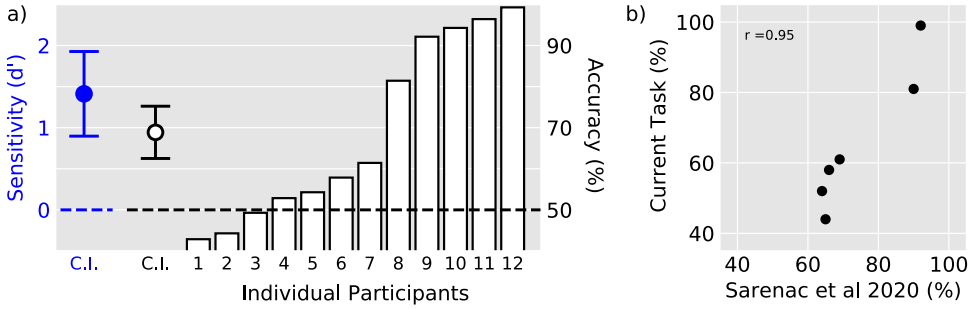

Figure 3. Group and individual-participant data. (**a**) Sensitivity and accuracy for the discrimination task. Each participant performed 140 trials over four days. The dashed lines indicate chance performance. The open bars illustrate individual rank-ordered performance, and the circular symbols illustrate group mean sensitivity (blue: left ordinate) and accuracy (black: right ordinate). The error bars are 95% confidence intervals. Generally, participants either performed very well or at chance levels. (**b**) Relationship between performance of common participants between Ref.[33] and the current study. Performance in the previous study was strongly predictive of performance in the current study.

spin-orbit states as described in Eq. (2). These two configurations possess uniform intensity profiles and were used during all experimental trials.

Seventeen participants were recruited in this study and provided informed written consent to voluntarily participate. All participants were treated in accordance with the Declaration of Helsinki, and all research activities received approval from the University of Waterloo Office of Research Ethics.

Before the main discrimination task, each participant performed an initial screening procedure in which a linearly polarized light beam was presented, whose polarization orientation rotated either clockwise or counterclockwise. Participants were presented with 10 testing trials and were asked to verbally discriminate the direction of rotation through the perception of rotating Haidinger's brushes. Twelve participants achieved > 70% accuracy and moved on to the main study. Participants performed the main discrimination task over four days, each containing thirty-five trials. Participants verbally discriminated between $|\Psi_+\rangle$ and $|\Psi_-\rangle$ configurations, and one randomly-selected configuration was presented per trial. All trials of the same type were identical to one another. See Supplementary Material C and D for full participation and psychophysical details, respectively.

Results

Participant performance was strikingly non-normal, and therefore non-parametric statistical tests were employed. No significant effect was found when subjecting the accuracy data from the 9 participants who scored less than 90% on the first day of the experimental task to a Friedman test with day as the repeated measure, $X^2(3) = 4.5$, $p = 0.22$. Therefore, the data from all days were collapsed for the main analysis. Sensitivity (d') and response bias (c) were calculated for each individual participant[56]. Accuracy (% correct) and sensitivity were analyzed using a one-tailed one-sample Wilcoxon signed rank test to determine whether group performance was significantly better than chance. Response bias was analyzed using a two-tailed one-sample Wilcoxon signed rank test to determine whether either response was systematically favored. Participants performed significantly better than chance: Median Accuracy = 60%, Median Sensitivity $d' = 0.5$, $W = 68$, $p = 0.01$ for both measures of performance. No significant response bias was observed: Median $c = 0$, $W = 42$, $p = 0.85$. Figure 3 illustrates group and single-subject data.

Discussion

Despite successful completion of our initial screening procedures from all participants (see Supplementary Material D for details), inspection of Fig. 3a reveals an evident bimodal distribution of task performance with subjects 1–7 performing at chance levels and subjects 8–12 performing at ceiling. One explanation for this pattern of results is that seven participants were unable to perform the relatively complex psychophysical task that required the combination of self-generated eye movements with judgements of Haidinger's brush orientation patterns. However, it is also possible that the bimodal distribution reflects individual differences in macular pigment structure[57–59]. Initial support for this intriguing possibility can be found in Ref.[33] where the same bimodal task performance distribution was observed for a much easier psychophysical task that employed a rotating beam and did not require self-generated eye movements. Figure 3b provides a visual comparison of both datasets for the six participants that completed both studies and confirms the robust nature of the bimodal performance distribution, demonstrating that performance in Ref.[33] was strongly predictive of performance in the current study. It is important to note that in both studies, each participant was initially required to demonstrate a strong ability to perceive Haidinger's brushes when viewing uniformly polarized light. Therefore, the stimuli and tasks employed by both studies are highly selective probes of sensitivity to the entoptic phenomenon. Our future studies will aim to gain further insights into the functional properties of individual macular pigment variations by examining the relationship between psychophysical performance and retinal images.

While the task employed in Ref.[33] may provide high resolution for capturing the full spectrum of spin-coupled OAM sensitivity, the current task appears exceedingly effective at identifying high and low spin-coupled OAM

discrimination performers, such that anybody unable to achieve ceiling performance will invariably perform near chance. Although both of these works have examined human perception of structured light that possess correlations between two degrees of freedom, protocols exist for the preparation of more complex spatial modes[60] and higher dimensional non-separable states[61]. An interesting future experiment to consider is the measurement of the classical GHZ state correlations using human detectors as per the polarization-based Bell-state projection measurements outlined in Ref.[61]. Furthermore, future work should apply these structured light discrimination tasks to measure properties of the macular pigment, allowing meaningful applications for diseases affecting the macular pigment such as macular degeneration[62–64].

Received: 11 August 2021; Accepted: 11 February 2022
Published online: 28 February 2022

References

1. Cohen, E. *et al.* Geometric phase from aharonov-bohm to Pancharatnam–Berry and beyond. *Nat. Rev. Phys.* **1**, 437–449 (2019).
2. Aharonov, Y. & Bohm, D. Significance of electromagnetic potentials in the quantum theory. *Phys. Rev.* **115**, 485 (1959).
3. Shivaramakrishnan, P. Generalized theory of interference, and its applications. In *Proceedings of the Indian Academy of Sciences-Section A*, Vol. 44, pp. 247–262. (Springer, Berlin, 1956).
4. Berry, M. V. The adiabatic phase and Pancharatnam's phase for polarized light. *J. Mod. Opt.* **34**, 1401–1407 (1987).
5. Wilczek, F. & Shapere, A. *Geometric Phases in Physics* Vol. 5 (World Scientific, 1989).
6. Berry, M. *et al.* Anticipations of the geometric phase. *Phys. Today* **43**, 34–40 (1990).
7. Bachtold, A. *et al.* Aharonov-bohm oscillations in carbon nanotubes. *Nature* **397**, 673–675 (1999).
8. Noguchi, A., Shikano, Y., Toyoda, K. & Urabe, S. Aharonov–Bohm effect in the tunnelling of a quantum rotor in a linear paul trap. *Nat. Commun.* **5**, 1–6 (2014).
9. Biener, G., Niv, A., Kleiner, V. & Hasman, E. Formation of helical beams by use of Pancharatnam–Berry phase optical elements. *Opt. Lett.* **27**, 1875–1877 (2002).
10. Hasman, E., Kleiner, V., Biener, G. & Niv, A. Polarization dependent focusing lens by use of quantized Pancharatnam–Berry phase diffractive optics. *Appl. Phys. Lett.* **82**, 328–330 (2003).
11. Bomzon, Z., Biener, G., Kleiner, V. & Hasman, E. Space-variant Pancharatnam–Berry phase optical elements with computer-generated subwavelength gratings. *Opt. Lett.* **27**, 1141–1143 (2002).
12. Marrucci, L., Manzo, C. & Paparo, D. Optical spin-to-orbital angular momentum conversion in inhomogeneous anisotropic media. *Phys. Rev. Lett.* **96**, 163905 (2006).
13. Nsofini, J. *et al.* Spin-orbit states of neutron wave packets. *Phys. Rev. A* **94**, 013605 (2016).
14. Sarenac, D. *et al.* Generation and detection of spin-orbit coupled neutron beams. *Proc. Natl. Acad. Sci.* **116**, 20328–20332 (2019).
15. Allen, L., Beijersbergen, M. W., Spreeuw, R. J. C. & Woerdman, J. P. Orbital angular momentum of light and the transformation of laguerre-gaussian laser modes. *Phys. Rev. A* **45**, 8185–8189 (1992).
16. Konrad, T. & Forbes, A. Quantum mechanics and classical light. *Contemp. Phys.* **60**, 1–22 (2019).
17. McLaren, M., Konrad, T. & Forbes, A. Measuring the nonseparability of vector vortex beams. *Phys. Rev. A* **92**, 023833 (2015).
18. Zhan, Q. Cylindrical vector beams: From mathematical concepts to applications. *Adv. Opt. Photon.* **1**, 1–57 (2009).
19. Cardano, F. *et al.* Polarization pattern of vector vortex beams generated by q-plates with different topological charges. *Appl. Opt.* **51**, C1–C6 (2012).
20. Galvez, E. J., Khadka, S., Schubert, W. H. & Nomoto, S. Poincaré-beam patterns produced by nonseparable superpositions of Laguerre-gauss and polarization modes of light. *Appl. Opt.* **51**, 2925–2934 (2012).
21. Rosales-Guzmán, C., Ndagano, B. & Forbes, A. A review of complex vector light fields and their applications. *J. Opt.* **20**, 123001 (2018).
22. Wang, X.-L., Ding, J., Ni, W.-J., Guo, C.-S. & Wang, H.-T. Generation of arbitrary vector beams with a spatial light modulator and a common path interferometric arrangement. *Opt. Lett.* **32**, 3549–3551 (2007).
23. Chen, H. *et al.* Generation of vector beam with space-variant distribution of both polarization and phase. *Opt. Lett.* **36**, 3179–3181 (2011).
24. Bomzon, Z., Kleiner, V. & Hasman, E. Pancharatnam–Berry phase in space-variant polarization-state manipulations with subwavelength gratings. *Opt. Lett.* **26**, 1424–1426 (2001).
25. Forbes, A. Controlling light's helicity at the source: Orbital angular momentum states from lasers. *Philos. Trans. R. Soc. A Math. Phys. Eng. Sci.* **375**, 20150436 (2017).
26. Oron, R. *et al.* The formation of laser beams with pure azimuthal or radial polarization. *Appl. Phys. Lett.* **77**, 3322–3324 (2000).
27. Rubinsztein-Dunlop, H. *et al.* Roadmap on structured light. *J. Opt.* **19**, 013001 (2016).
28. Milione, G. *et al.* 4× 20 gbit/s mode division multiplexing over free space using vector modes and a q-plate mode (de) multiplexer. *Opt. Lett.* **40**, 1980–1983 (2015).
29. Marrucci, L. *et al.* Spin-to-orbital conversion of the angular momentum of light and its classical and quantum applications. *J. Opt.* **13**, 064001 (2011).
30. Arora, G., Deepa, S., Khan, S. N. & Senthilkumaran, P. Detection of degenerate stokes index states. *Sci. Rep.* **10**, 1–10 (2020).
31. Angelsky, O. V., Mokhun, I. I., Mokhun, A. I. & Soskin, M. S. Interferometric methods in diagnostics of polarization singularities. *Phys. Rev. E* **65**, 036602 (2002).
32. Giordani, T. *et al.* Machine learning-based classification of vector vortex beams. *Phys. Rev. Lett.* **124**, 160401 (2020).
33. Sarenac, D. *et al.* Direct discrimination of structured light by humans. *Proc. Natl. Acad. Sci.* **117**, 14682–14687 (2020).
34. Tinsley, J. N. *et al.* Direct detection of a single photon by humans. *Nat. Commun.* **7**, 12172 (2016).
35. Loulakis, M., Blatsios, G., Vrettou, C. S. & Kominis, I. K. Quantum biometrics with retinal photon counting. *Phys. Rev. Appl.* **8**, 044012 (2017).
36. Sim, N., Cheng, M. F., Bessarab, D., Jones, C. M. & Krivitsky, L. A. Measurement of photon statistics with live photoreceptor cells. *Phys. Rev. Lett.* **109**, 113601 (2012).
37. Dodel, A. *et al.* Proposal for witnessing non-classical light with the human eye. *Quantum* **1**, 7 (2017).
38. Margaritakis, A., Anyfantaki, G., Mouloudakis, K., Gratsea, A. & Kominis, I. K. Spatially selective and quantum-statistics-limited light stimulus for retina biometrics and pupillometry. *Appl. Phys. B Lasers Opt.* **126**, 20 (2020).
39. Karnieli, A., Li, Y. & Arie, A. The geometric phase in nonlinear frequency conversion. *Front. Phys.* **17**, 1–31 (2022).
40. Shen, Y. Rays, waves, su (2) symmetry and geometry: Toolkits for structured light. *J. Opt.* **23**, 124004 (2021).
41. Haidinger, W. Ueber das directe erkennen des polarisirten lichts und der lage der polarisationsebene. *Ann. Phys.* **139**, 29–39 (1844).
42. Misson, G. P., Timmerman, B. H. & Bryanston-Cross, P. J. Human perception of visual stimuli modulated by direction of linear polarization. *Vis. Res.* **115**, 48–57 (2015).

43. Misson, G. P. & Anderson, S. J. The spectral, spatial and contrast sensitivity of human polarization pattern perception. *Sci. Rep.* **7**, 16571 (2017).
44. Misson, G. P., Temple, S. E. & Anderson, S. J. Computational simulation of human perception of spatially dependent patterns modulated by degree and angle of linear polarization. *JOSA A* **36**, B65–B70 (2019).
45. Horváth, G., Horváth, G. & Varju, D. *Polarized Light in Animal Vision: Polarization Patterns in Nature* (Springer, 2004).
46. Temple, S. E. *et al.* Perceiving polarization with the naked eye: Characterization of human polarization sensitivity. *Proc. R. Soc. B Biol. Sci.* **282**, 20150338 (2015).
47. Bone, R. A. The role of the macular pigment in the detection of polarized light. *Vis. Res.* **20**, 213–220 (1980).
48. Coren, S. The use of Haidinger's brushes in the study of stabilized retinal images. *Behav. Res. Methods Instrum.* **3**, 295–297 (1971).
49. Berry, M. V. Optical vortices evolving from helicoidal integer and fractional phase steps. *J. Opt. A Pure Appl. Opt.* **6**, 259 (2004).
50. Sarenac, D. *et al.* Generation of a lattice of spin-orbit beams via coherent averaging. *Phys. Rev. Lett.* **121**, 183602 (2018).
51. Schwarz, S. *et al.* Talbot effect of orbital angular momentum lattices with single photons. *Phys. Rev. A* **101**, 043815 (2020).
52. Sarenac, D. *et al.* Methods for preparation and detection of neutron spin-orbit states. *New J. Phys.* **20**, 103012 (2018).
53. Furukawa, A. *et al.* Effective speckle reduction in laser projection displays. In *Emerging Liquid Crystal Technologies III* Vol. 6911 (ed. Chien, L.-C.) 183–189 (International Society for Optics and Photonics (SPIE), 2008).
54. Schaefer, B., Collett, E., Smyth, R., Barrett, D. & Fraher, B. Measuring the stokes polarization parameters. *Am. J. Phys.* **75**, 163–168 (2007).
55. InternationalÃ‚Â Commission onÃ‚Â Non-Ionizing RadiationÃ‚Â Protection. Revision of guidelines on limits of exposure to laser radiation of wavelengths between 400 nm and 14 μm. *Health Phys.* **79**, 431–440 (2000).
56. Wickens, T. D. *Elementary Signal Detection Theory* (Oxford University Press, 2002).
57. De Vries, H. L., Spoor, A. & Jielof, R. Properties of the eye with respect to polarized light. *Physica* **19**, 419–432 (1953).
58. Liebman, P. A., Jagger, W. S., Kaplan, M. W. & Bargoot, F. G. Membrane structure changes in rod outer segments associated with rhodopsin bleaching. *Nature* **251**, 31–36 (1974).
59. Hochheimer, B. F. & Kues, H. A. Retinal polarization effects. *Appl. Opt.* **21**, 3811–3818 (1982).
60. Shen, Y., Wang, Z., Xing, F., Naidoo, D. & Forbes, A. Su (2) poincaré sphere: A generalized representation for multidimensional structured light. *Phys. Rev. A* **102**, 031501 (2020).
61. Shen, Y. *et al.* Creation and control of high-dimensional multi-partite classically entangled light. *Light Sci. Appl.* **10**, 1–10 (2021).
62. Forster, H. W. The clinical use of the haidinger's brushes phenomenon. *Am. J. Ophthalmol.* **38**, 661–665 (1954).
63. Naylor, E. J. & Stanworth, A. The measurement and clinical significance of the Haidinger effect. *Trans. Ophthalmol. Soc. U.K.* **75**, 67 (1955).
64. Müller, P. L. *et al.* Perception of haidinger brushes in macular disease depends on macular pigment density and visual acuity. *Investig. Ophthalmol. Visual Sci.* **57**, 1448–1456 (2016).

Acknowledgements

This work was supported by the Canadian Excellence Research Chairs (CERC) program, the Natural Sciences and Engineering Research Council of Canada (NSERC) Grants [RGPIN-2018-04989], [RPIN-05394], [RGPAS-477166], the Collaborative Research and Training Experience (CREATE) program, the Government of Canada's New Frontiers in Research Fund (NFRF) [NFRFE-2019-00446], the Velux Stiftung Foundation [Grant 1188], and the Canada First Research Excellence Fund (CFREF).

Author contributions

D.S., A.E.S., C.K., D.G.C., and D.A.P. designed and constructed and optimized the optical setup. A.E.S. and B.T. designed the psychophysical study. D.S., C.K., and A.E.S. carried out the study. A.E.S. and B.T. analyzed the results. All authors contributed to writing the paper.

Competing interests

The authors declare no competing interests.

Additional information

Supplementary Information The online version contains supplementary material available at https://doi.org/10.1038/s41598-022-07089-4.

Correspondence and requests for materials should be addressed to D.S.

Reprints and permissions information is available at www.nature.com/reprints.

Publisher's note Springer Nature remains neutral with regard to jurisdictional claims in published maps and institutional affiliations.